SERI/TR-8041-14-T1
(DE82017203)

POLYCRYSTALLINE SOLAR CELL/SUBSTRATE GROWTH BY INTEGRATED VACUUM EVAPORATION

Period of Performance: September 25, 1979—June 25, 1981

By
Donald L. Smith

February 1982

Work Performed Under Contract No. AC02-77CH00178

Perkin-Elmer Corporation
Norwalk, Connecticut

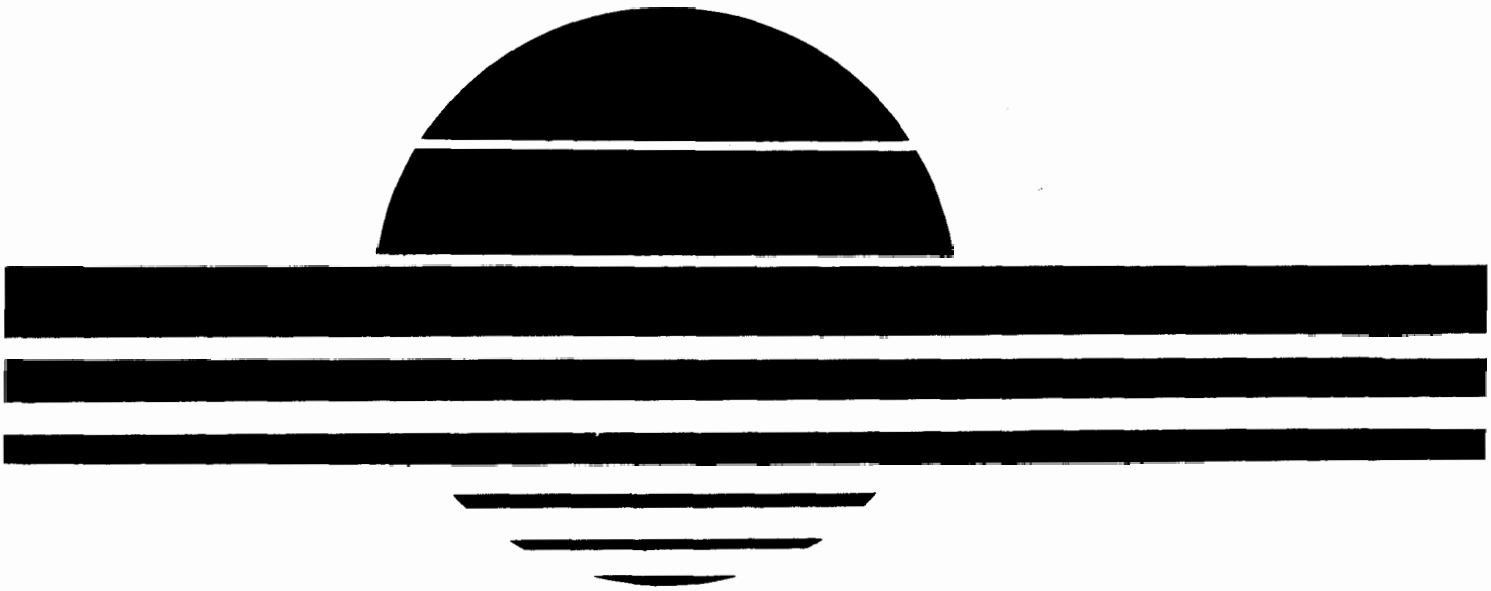

U.S. Department of Energy

Solar Energy

DISCLAIMER

This report has been reproduced directly from the best available copy.

Available from the National Technical Information Service, U. S. Department of Commerce, Springfield, Virginia 22161.

Price: Printed Copy A03
Microfiche A01

Codes are used for pricing all publications. The code is determined by the number of pages in the publication. Information pertaining to the pricing codes can be found in the current issues of the following publications, which are generally available in most libraries: *Energy Research Abstracts, (ERA); Government Reports Announcements* and Index (*GRA* and I); *Scientific and Technical Abstract Reports (STAR);* and publication, NTIS-PR-360 available from (NTIS) at the above address.

SERI/TR-8041-14-T1
(DE82017203)
Distribution Category UC-63b

POLYCRYSTALLINE SOLAR CELL/SUBSTRATE GROWTH BY INTEGRATED VACUUM EVAPORATION

Final Report

February, 1982

Period of Performance: September 25, 1979 - June 25, 1981

Principal Investigator: Donald L. Smith

SERI Subcontract No. XS-9-8041-14

Perkin-Elmer Corporation
Norwalk, Connecticut 06856

ABSTRACT

GaAs epitaxy on a large-grained substrate would reduce grain-boundary shunting losses in polycrystalline solar cells. In pre-contract work, Fe was selected for its low cost and 1.4% lattice match, and was e-beam evaporated onto 850-1100°C alumina and Kovar wafers, selected for reasonably good thermal expansion match to GaAs. Fe films developed 30-200 μm grains with a (211) texture and did not crack or peel upon cooldown. Under the contract, clean, single-crystal Fe surfaces for GaAs growth studies were generated by epitaxial growth of Fe onto 300°C GaAs(211); but the reverse process, GaAs growth on Fe (by vacuum deposition from Ga and As_4) produced polycrystalline Ga-As-Fe mixed phases. The success of Fe epitaxy on GaAs is attributed to the availability of Ga and As at the interface only as the compound GaAs, which raises the activation energy for the formation of mixed phases. Fe passivation by NH_3 and H_2S exposure was tried unsuccessfully, although H_2S did passivate Fe against As_4. Various closely lattice-matching materials were vacuum-deposited on the Fe as "buffer" layers prior to GaAs growth. AlAs and Ge formed mixed phases with the Fe. Cr grew epitaxially because Cr and Fe are both bcc, but deposition of GaAs and of Ge on the Cr produced mixed phases. SrF_2 did grow epitaxially on Fe, and this was attributed to its existence as a molecule in the vapor. GaAs grew epitaxially on a 0.5 μm-thick buffer layer of SrF_2 on Fe, and electrical conductivity was observed between the GaAs and the Fe, apparently through microvoids in the facetted SrF_2 epilayer.

ACKNOWLEDGEMENTS

Many people provided helpful suggestions or assistance during the course of the work, especially Richard Bruce, Ron Bunshah, Don Feucht, Art Gossard, Andrew McCullough, Dave Miller, Matt Miller, Dale Partin, Dick Stirn, and Colin Wood. Expert technical assistance was provided by Mike Pascarella, Vince Pickhardt, and Paul Saviano.

TABLE OF CONTENTS

INTRODUCTION

GaAs is an attractive solar cell material because its 1.4 eV bandgap is well-matched to the solar spectrum and because its optical absorption coefficient is compared to indirect-bandgap materials like Si, so that only 1-2 μm of depth is needed to collect most of the sunlight. The shallow collection depth reduces the minority carrier diffusion length required for efficient collection, given a shallow-junction cell(1), and also makes conceivable an inexpensive cell, despite the high cost of Ga, by using thin GaAs grown on an inexpensive substrate. Unfortunately, polycrystalline GaAs cells grown on such substrates have exhibited serious grain-boundary shunting. This has been counteracted by growing thicker films to achieve a proportionate increase in grain size, and by employing various grain-boundary passivating treatments(2,3). Nevertheless, the GaAs thickness required to achieve reasonable cell efficiency is still much larger than the sunlight absorbtion depth(4,5), and the cost of this extra Ga is significant.

Grain boundary effects could be reduced without using excess GaAs by growing films with grains much wider than the film thickness. One way to achieve this is to grow the GaAs epitaxially on the individual grains of an inexpensive large-grained substrate. The following criteria must be considered in the choice of such a substrate:

1) Low cost, in the thickness required to achieve sufficient grain size.
2) Low crystallographic lattice constant mismatch, Δa, to GaAs.
3) Low mismatching thermal expansion coefficent α, to GaAs.
4) Low vapor pressure at the GaAs growth temperature.
5) Melting point higher than the GaAs growth temperature.
6) Electrical conductivity sufficient for negligible series resistance.
7) Ohmic contact to GaAs.
8) Surface sufficiently clean for epitaxy.

9) Noncontaminating to bulk of GaAs film.

10) Nonreactive with depositing GaAs at the growth temperature.

Ge satisfies all but the cost criterion, which has recently been overcome by growing Ge on Si(100) by vacuum evaporation. Shallow homojunction GaAs cells on the substrate(6) have shown efficiences up to 12% despite the 3.9% Δa of Si to GaAs, making this a promising system for polycrystalline GaAs solar cells provided that similar film quality becomes obtainable on planes other than (100). The approach pursued in the present work to satisfy the above ten criteria centers around the fact that many metallic elements can be vacuum-evaporated into smooth, large-grained films on amorphous substrates held at sufficiently high temperature(7). Although no metallic elements satisfy both criteria 2 and 3, a metal having low Δa to GaAs, grown on a much thicker support material having good α match to GaAs, would expand and contract with the substrate, thus satisfying both criteria. Cr and Fe have low Δa's to GaAs, +2.0 and +1.4% respectively, and also satisfy criteria 1,4,5, and 6. It will be shown in Section II that Fe with large, smooth grains can be evaporated onto materials having α's close to that of GaAs. The films remain adherent and continuous after cooldown despite the α mismatch strain.

The surface of clean evaporated Fe would instantly become contaminated in air during transfer to a GaAs grower, because of its high reactivity. However, the sequential growth of Fe and GaAs in the same vacuum would insure satisfaction of criterion 8. While the growth of GaAs by vacuum evaporation, or molecular beam epitaxy (MBE), is not generally thought of as a low-cost process, this is largely because of its historical development as a small-scale research tool. The advent of closed-cycle He cryopumping has greatly simplified the achievement of large-scale (3-meter) ultra-high vacuum, and the use of H_2 background to scavenge C and O has lowered the vacuum requirements for obtaining good GaAs(8). Excellent GaAs junction solar cells have been grown by MBE on single-crystal GaAs(9) and Ge(10). Alternatively, the Fe could be protected by a less easily contaminated "buffer layer" coating (see Section III) during transfer to a CVD GaAs grower.

With regard to ohmic contacts (criteron 7), these amount to tunneling contacts for GaAs, because of Fermi level pinning near midgap by interface states; doping levels over about $10^{19}/cm^3$ make the depletion width narrow enough so that tunneling conduction is effectively ohmic (11). These levels can be achieved without alloying in MBE growth using Be(12) or ionized Zn(13) for p-type and Sn(14) or SnSe(15) for n-type dopants. In our laboratory, Fe evaporated onto 500°C, 1 x 10^{19}/ cm^3-doped p- and n-GaAs resulted in contact resistance $\leq 10^{-3}$ Ω-cm^2 in pre-contract studies.

With regard to bulk contamination of the GaAs film by Fe (criteron 9), Fe is believed to act as a deep acceptor in GaAs(16). However, the extent of its penetration into an epitaxial film grown on Fe depends on the time-temperature conditions accompanying the growth of the film. There is evidence that penetration would not be significant under conditions anticipated here, especially if MBE were used, since it takes place at relatively low temperature. Diffusion of Fe into n-GaAs for 5 minutes at 500°C actually increases minority carrier diffusion length, possibly due to Ga vacancy filling(17). The use of a "buffer layer" on the Fe (see Section III) would reduce Fe penetration still further.

The one remaining criterion (no. 10) has so far not proved possible to satisfy by the direct growth of GaAs on Fe. Chemical interactions between Ga and Fe and/or As and Fe produce undesired phases which destroy the epitaxy. However, it will be shown in Section III that this problem can be overcome by the incorporation of an appropriate "buffer layer," grown epitaxially on the Fe before GaAs growth. The polycrystalline GaAs/Fe system appears, therefore, to be a promising candidate for high-efficiency, low-cost solar cells.

II. SUBSTRATE GROWTH*

Many metals grow into large (>20 μm), columnar preferentially-oriented grains when vacuum-deposited onto substrates held near ½ the

*These studies of the growth, by electron-beam evaporation, of polycrystalline Cr and Fe substrates were carried out prior to the subject contract, but are included here for the sake of completeness in the discussion of our overall approach.

absolute-temperature melting point (mp) and into even larger but more randomly-oriented grains at higher temperature(7). In our laboratory, 4-nines pure Cr and 3-nines Fe were e-beam evaporated in a 10^{-3}-10^{-4} Pa vacuum onto 1 mm-thick substrates held at various temperatures. Substrates, chosen for α near that of GaAs (6×10^{-6}/°C), included Kovar (5×10^{-6}) and alumina (7×10^{-6}); by comparison, Fe has an α of 12×10^{-6}. Both substrates were polished to <1 μm roughness to minimize substrate influence on film surface topography.

We were unable to obtain large-grained, dense Cr films by this technique. Deposits 25-50 μm thick on alumina at 800°C (= 0.49 mp) and at 1050°C, even after 1 hour of annealing, produced only randomly-oriented, loosely-connected square platelets 1 to 2 μm in diameter. Similarly small grains and porous structure have been obtained by others (18,19).

Fe films did develop the desired grain structure. 80 μm-thick films grown at about 1 μm/min. on 850°C Kovar had 28 μm average grain width at the surface, and films were generally smooth to 0.2 μm as determined both by scanning electron microscopy cleaved cross-sections and by optical interference microscopy of the surface. Grain structure was columnar and void-free. Films grown at 14 μm/min. had 10 μm grain width, but this increased to 30 μm after a 1½ hour anneal at the growth temperature. Shorter anneals were not tried, and might have produced the same results. Similar grain size at the same growth temperature was obtained on alumina, although film surfaces were rougher, possibly due to selective nucleation on the ½ to 3 μm grains of the alumina. On 1100°C alumina, grain width ranged from 60-200 μm. Above 910°C, Fe changes phase from body-centered cubic (α-Fe or ferrite) to face-centered cubic (γ-Fe, or austenite), so the 1100°C film would have grown as γ-Fe, but X-ray analysis showed that it had transformed completely to α-Fe upon cooldown. The fraction of retained austenite after cooldown in general depends on the quenching rate and the amount and type of impurities present(20). α-Fe is the phase whose lattice constant matches that of GaAs. The above result shows that very large grain size can be obtained by growing well above the phase transition temperature without losing the desired α-Fe structure after cooldown. Occasionally, an

array of pillars or edgewise-oriented ribbons developed on the Fe surface, but the cause of these was not identified. Even in the case of films deposited at the highest temperature (1100°C), no peeling or cracking was observed after cooldown despite the thermal mismatch strain of about ½%, which may have partially annealed out during cooldown.

A detailed picture of the growth of grain diameter with film thickness was obtained for one film by angle-lapping and etching for 10 seconds in 5% HNO_3/methanol to bring out the grain structure. The 40 μm-thick film used had been grown at 5 μm/min. on 880°C alumina. The result (Figure 1) shows a rapid increase in grain diameter from the substrate up to 4 μm of film thickness, after which it levels out. The average grain diameter at the surface of this film is 37 μm. Grain diameter growth with thickness is believed to involve a process of closing out of less favorably oriented (from a thermodynamic standpoint) grains by those more favorably oriented, resulting in a preferential crystallographic texture normal to the surface(7). This texture was examined by plotting X-ray pole figures(21) for films grown at 750 and 1100°C on alumina. The 750°C films showed a strong (211) texture with a possible (111) component, both being rotationally symmetric about the film surface normal. The 1100°C film had a similar texture with an additional (311) component. Comparable grain size vs. temperature has been reported for Fe e-beam evaporated onto 530-1100°C stainless steel; but while grain texture was predominantly (211) at the lower temperature, it became more (110) at the higher, and was random for depositions made above the $\alpha \rightarrow \gamma$ phase transition temperature(22).

III. GaAs HETEROEPITAXY

It will be seen below that while Fe could be grown on GaAs epitaxially, GaAs on Fe could not. The use of various potentially epitaxial vacuum-evaporated buffer layers was examined for the purpose of blocking the apparent chemical interaction between Fe substrates and depositing Ga and As_4. Materials tried included AlAs, Ge, Cr, and SrF_2, the last having been successful. Fe passivation by exposure to NH_3 and H_2S was also examined.

A. Experimental Procedures

Clean, single-crystal Fe substrates for growth studies were generated within the epilayer growth vacuum by evaporation of a 0.1 μm epitaxial layer of Fe onto single-crystal GaAs wafers. In this way, hereroepitaxy could be studied without the complication of the grain structure and topography of the Fe substrates whose growth was discussed in Section II. While the thick Fe films of Section II required e-beam evaporation, it was found possible to evaporate the 0.1 μm layers from a tungsten-coil-heated crucible of the usual MBE design, which could be much more easily incorporated into the GaAs growth system.

All growths were carried out in an MBE system whose basic features have been described previously(23), although various modifications have been made subsequently as described in Appendix A. In the present work, substrates were injected through a load-lock onto a linear positioner, as shown in Figure 3, Appendix A. The positioner first entered the analytical chamber, which contained retarding-grid electron optics for low-energy electron diffraction (LEED) and Auger analysis, and then entered the MBE growth chamber. The GaAs and also the AlAs and Ge buffer layers were grown from the pure elements within the LN_2-shrouded MBE chamber, while the Fe substrates and the SrF_2 and Cr buffer layers were evaporated within in-line appendages in the analytical chamber from sources having water-cooled shrouds. Fe and SrF_2 were evaporated from alumina crucibles and Cr from standard electroplated tungsten rods. All deposition rates were calibrated with room-temperature quartz crystal microbalances, including that of As_4 by using enough Ga codeposition to raise its sticking coefficient to unity. Deposition rates were generally ½ to 1½ μm/hr.

The GaAs wafers were In-wetted to a Mo block which could be temperature-controlled at any station of the linear positioner. Chemicall y-polished GaAs wafers were cleaned by conventional procedures: degreasing, immersing for 2 minutes in an etch of $1H_2O + H_2O_2 + 7H_2SO_4$, and heating to 600°C in the growth vacuum under an As_4 beam flux of 1×10^{15} molecules/cm^2-sec.

NH_3 and H_2S exposures were carried out in the analytical chamber. Pressures were monitored on a bakable capacitance manometer.

Derivative Auger spectra were always taken with a 2.5 KV, 50 μA beam and 10 V_{pp} grid modulation to facilitate peak height comparisons among a series of spectra.

In preparation for the processing of GaAs solar cells on Fe, "baseline" solar cells were first grown on single crystal n^+-GaAs substrates to provide a standard of comparison. These were Au Schottky-barrier cells on MBE n-GaAs. Their growth, processing, and electrical characterization are described in detail in Appendix B.

B. Fe-GaAs Heteroepitaxy

Fe was grown epitaxially on GaAs (110), (111), and (211); the last plane was used the most, since it is the preferred orientation of our polycrystalline Fe. Epitaxy was obtained even on 25°C wafers, as evidenced by a symmetric array of bright LEED beams and a low level of diffuse background glow, although beams were relatively broad compared to those typical of well-ordered crystals, indicating considerable strain. For 600°C growth, beams were sharp but were "maverick"; that is, they did not converge radially with increasing electron energy, indicating an Fe surface reconstructed into facets, or pyramids. Those surfaces were also visibly rough. 300°C deposition gave surfaces mirror-smooth to the eye with sharp, low-background LEED patterns containing no maverick beams. Fe grown at this temperature was used for all studies reported below. Epitaxy of evaporated Fe on GaAs has also been reported by other laboratories(24,25).

The behavior of the reverse process GaAs growth on Fe, was very different. Results are summarized in Table I. No LEED pattern appeared for growth temperatures of 400-600°C, and surfaces were very rough. An incident As_4/Ga molecular ratio of 2 was usually used, although 20 was also tried at 460 and 600°C. Thinner films at higher temperatures showed some Fe in the Auger spectrum, as shown in Table I. This signal could have arisen either from Fe diffusion through the deposit or from

bare areas of substrate between pyramids of reconstructed deposit. Exposure of the Fe to the As_4 beam alone for only a few seconds within this temperature range also resulted in complete removal of the LEED pattern: polycrystalline Fe-As phases are presumably forming. Ga-Fe liquid alloys might also be forming during Ga and As_4 co-deposition.

C. Fe Passivation

It has been reported that nitridation of single-crystal Fe in amounts small enough to retain the Fe reflection electron diffraction pattern can offer significant protection against corrosion in moist air(26). We found that Fe nitridation in NH_3 at 450°C could be continued up to a N/Fe Auger peak ratio of about 1.4 μV/2.8 μV without degrading the LEED pattern. (The clean Fe Auger peak height at 651 eV was 3.7 μV.) No attempt was made to relate the N Auger peak height to fractional surface coverage. The above amount of nitridation was obtained for a 10 sec. exposure to 1×10^5 Pa (1 atm.) of NH_3. For a given exposure, higher temperature resulted in less N coverage and lower resulted in more. However, subsequent exposure to the As_4 beam for only 5 sec. at 450°C resulted in removal of the LEED pattern and almost complete displacement of N by As in the Auger spectrum. NH_3 treatments are summarized in Table IV.

Passivation by sulfidation was considered because the pyrite phase of FeS_2 is a reasonable lattice match to GaAs ($\Delta a = 4.4\%$). Growth of an FeS_2 buffer layer onto Fe was tried first, by two techniques, but was unsuccessful. Growth by evaporation of FeS_2 powder released only S into the vapor. For growth by reactive evaporation, Fe deposition from a pure Fe source was monitored with the quartz crystal microbalance as a 5×10^{-2} Pa background of H_2S was introduced: no significant increase in deposition rate was observed, so it was concluded that the reaction to FeS_x was not proceeding at a significant rate. Nevertheless, considerable sulfidation of a clean Fe substrate surface could be obtained by exposure to H_2S gas. A good LEED pattern remained up to a S/Fe Auger peak ratio of about 40 μV/2.5 μV, which was obtained for a 10 sec. exposure to 13 Pa of H_2S at 450°C. As in the case of NH_3, higher temperatures resulted in less sulfidation, and fractional S coverage was

not calibrated. The sulfided surface did offer some protection against reaction with the As_4 beam. While a 5 sec. exposure of clean or nitrided Fe to the As_4 beam had completely removed the LEED pattern, the same exposure of the sulfided Fe to it at 450°C resulted in only slight pattern degradation. However, GaAs grown at 450°C and 550°C on surfaces so prepared gave no LEED pattern. H_2S treatments are summarized in Table IV.

D. Buffer Layer Growth

Table I summarizes results for the growth on Fe of various buffer layers, including AlAs, Ge, Cr, and SrF_2, all of whose lattice constants match that of GaAs to $\cong$ 2% or less. The search for potential buffer layers was limited to cubic materials, since those with other symmetries would match only on specific crystallographic planes and therefore would not be suitable for epitaxy on polycrystalline substrates. Many closely lattice-matching materials were eliminated on the basis of excessive vapor pressure (>10^{-4}Pa) at the anticipated minimum GaAs growth temperature of 500°C, including PbS, NaCl, CuBr, Sb_2O_3, and MoO_3. Aside from AlAs, dissociatively evaporating compounds like ZnSe and CuS were not tried despite their satisfying the other criteria, for reasons discussed in Section E below.

In preparation for the growth of AlAs of Fe, AlAs epitaxy was demonstrated on GaAs (as evidenced by sharp, symmetrical LEED patterns) at 1 μm/hr. and incident As_4/Ga ratios of 10 and 2 over a substrate temperature range of 350-600°C. Depositions under the same conditions onto 400 and 600°C Fe gave no LEED patterns, and surfaces were visibly rough. Fe appeared in the Auger spectrum of a 400°C film 0.05 μm thick, but not in one 0.3 μm thick, as shown in Table I. This behavior is similar to that for the growth of GaAs on Fe.

Ge was grown epitaxially on 400°C GaAs at 0.7 μm/hr. On Fe, two Ge growth regimes were observed as substrate temperature was varied. From 430 to 600°C, LEED patterns were observed for films 0.1 to 0.9 μm thick, but weakened with increasing thickness, and considerable Fe appeared in

the Auger spectrum of a 500°C film 0.1 μm thick. From 300 to 400°C, no Fe appeared in the Auger spectrum of 0.1 μm films, but there was no LEED pattern either. All depositions were visibly rough. This evidence suggests that below 400°C uniform polycrystalline Ge is forming, while above 400°C polycrystalline Ge or Ge-Fe is forming in islands which finally both coalesce and become buried by Ge. The LEED pattern comes from the exposed Fe substrate between the islands, and this area disappears with increasing film thickness.

Cr grown on Fe at 400 and 600°C gave sharp, bright, low-background, unfacetted LEED patterns, despite the presence of 0.7 μV of Fe in the Auger spectrum of a 600°C film 0.06 μm thick. For GaAs growth studies, Cr was grown at 400°C to a greater thickness of 0.2-0.3 μm to attenuate this Fe out-diffusion. The rate of Fe out-diffusion was estimated by annealing a 0.1 μm thick Cr film on Fe at 550°C: after 30 sec., Fe began to appear in the Auger spectrum (0.2 μV peak height, compared to 3.7 μV for pure Fe). GaAs grown on the Cr/Fe over a temperature range from 400-560°C gave no LEED pattern, and the amount of Cr appearing in the GaAs Auger spectrum increased with increasing growth temperature, as shown in Table I. These results are similar to those for GaAs/Fe. On the premise that it was the As_4 which was preventing epitaxy, a special growth procedure was then tried which consisted of a 2.5 min. predeposition of Ga alone at 25°C followed by 3½ min. of As_4 alone at the GaAs growth temperature, using the same beam fluxes as for the usual GaAs growth at 1 μm/hr. and $As_4/Ga = 2$. This nucleation step was followed by GaAs growth in the usual manner. The objective was to prevent Fe from seeing As until the As had reacted with Ga. Tried first on GaAs, the procedure gave epitaxial GaAs at growth temperatures from 400-500°C, but on Cr/Fe at the same temperatures no LEED patterns were observed. It appears, therefore, that the Ga as well as the As is interacting with the Cr.

Ge was also grown on the above Cr/Fe substrates, the Cr being used as a buffer to block Ge-Fe interaction and the Ge to block GaAs-Cr interaction. However, Ge grown at 300, 400, and 500°C gave no LEED pattern. 0.1 μm films grown at the highest temperature contained 2.2 μV

Cr in the Auger spectrum at 529 eV (compared to 7.5 μV for pure Cr), while the others contained none.

In contrast to the above negative results, it was found that SrF_2 could be grown epitaxially on Fe at 400 and 600°C. LEED showed facetting, and Fe appeared in the Auger spectra of 0.1 μm-thick but not of 0.5 μm-thick films. This Fe signal apparently arose from clear Fe areas between islands of SrF_2, islands which coalesce after 0.5 μm of growth. While GaAs grew polycrystalline on the thinner SrF_2, it was epitaxial on the thicker at both 540 and 600°C; LEED indicated facetting of the GaAs at 600°C. A 2.5 μm-thick GaAs film grown at 540°C showed LEED quality equivalent to that for GaAs on GaAs in terms of LEED beam sharpness and background level. Most of this film was visibly rough, but there were some shiny patches. Although SrF_2 is of course an insulator, the GaAs film could not be electrically isolated from the Fe for resistivity measurement, even when scribed through to the substrate all around the periphery. Au contact pads were evaporated onto the GaAs, and probing from these to the Fe subtrate showed some back-to-back diodes and some ohmic contacts on the order of 0.5 Ω-cm^2, on both the shiny and the rough areas of this unintentionally-doped film. Conduction might be occurring through pinholes in the SrF_2 between barely-coalesced islands. If so, an optimum SrF_2 buffer layer thickness might exist which would be thick enough to insure high-quality epitaxy yet thin enough to avoid excessive cell series resistance.

E. Discussion

The vacuum-deposited species (Ga + As_4), (Al + As_4), and Ge all appear to form mixed phases with Fe substrates which prevent heteroepitaxial growth by MBE. On the other hand, Cr and SrF_2 can be grown epitaxially on Fe, and Fe can be grown epitaxially on GaAs. The fact that Fe can be grown on GaAs but GaAs cannot be grown on Fe is likely to be due to the presence of only the compound (GaAs) at the interface in the former case, but of the elements Ga and As as well in the latter case. The activation energy for the formation of Ga-Fe and As-Fe phases would be expected to be much larger in the former case because of the

need to break the Ga-As bond in the course of their formation. Even though equilibrium may favor the formation of mixed phases between a GaAs substrate and depositing Fe, the process proceeds slowly enough, at the Fe growth temperature of 300°C, so that a smooth epitaxial film of Fe can be formed before new phases appear to a noticeable degree. But in GaAs and AlAs growth on Fe, mixed phases form rapidly between the depositing elements and the Fe before an epilayer of GaAs or AlAs can be nucleated. A similar difference in degree of difficulty of epitaxial growth has been encountered in the MBE growth of Ge on GaAs vs. GaAs on Ge(28), although smooth epitaxial GaAs on Ge has now been achieved(29, 30). It is important to note that while mixed phase formation in the growth of Ge on GaAs is slow enough so as not to interfere with epitaxy, it does proceed and can be detected by X-ray photoelectron spectroscopy(31). It has also been suggested(32) that the greater difficulty of GaAs on Ge growth relative to Ge on GaAs is due to the increased number of defects such as antiphase boundaries which are possible in the more complex crystal structure of the compound.

The mixed-phase problem is likely to appear in the growth by MBE of any dissociatively-evaporating compound on an elemental substrate, due to competing element-element reactions at the interface. Consequently, other dissociatively-evaporating potential buffer layer materials, such as ZnSe and CuS, were not considered in this work despite favorable lattice matches. On the other hand, SrF_2 almost certainly evaporates nondissociatively because of its strong ionic bond, so that its elements are not available for reaction with Fe, and epitaxy proceeds unimpeded. Nondissociative evaporation has been confirmed by mass spectroscopy for CaF_2 and BaF_2 during epitaxial growth on various semiconductors(33).

Mixed phases also appear to form during the growth of elemental Ge on Fe, even though the eutectic temperature is 850°C(34), well above the growth temperature used here. Rapid solid-state interdiffusion is presumably occurring, as is the case when Ge is grown on GaAs at too high a temperature(31). Cr epitaxy on Fe is a special case in which mixed phases can be avoided, because both elements are body-centered cubic and form a continuous solid solution over the entire composition

range; the one intermediate phase which has been reported (σ) forms extremely slowly even at 600°C(34). A similar situation exists for Ge and Si, for which there are no intermediate phases, and MBE of Ge on Si has been demonstrated, as noted in Section I(6).

The generalized heteroepitaxial growth condition is illustrated in Figure 2 by a plot of activation energy for the formation of mixed phases (E_a) vs. growth temperature (T). For a given growth rate, there will be a minimum growth temperature for epitaxy (T_e) below which films will be polycrystalline or amorphous, even though mixed phases might not be forming, because a certain amount of energy is required for structure propagation. In heteroepitaxial growth situations for which the formation of mixed phases at the interface is thermodynamically favorable, the temperature above which such mixed phases form rapidly enough to destroy epitaxy will increase with E_a, as shown by the curve. If E_a is above the critical value E_c shown in Figure 2, there will be a finite temperature range over which heteroepitaxy is possible: if it is below, there will not. The width of this "window" also may depend somewhat on growth rate. The results reported in the present work suggest that the window is very wide for Fe on GaAs, for GaAs on SrF_2, and for SrF_2 on Fe, because of high E_a's, and that it may not exist for GaAs, AlAs, and Ge on Fe or Cr.

IV. CONCLUSIONS

GaAs growth on SrF_2/Fe appears to be a viable approach to achieving a large ratio of grain width to thickness on an inexpensive substrate. Large-grained Fe deposits remain adherent to support wafers whose thermal expansion coefficients are close to that of GaAs, thus forming a closely lattice-and thermal-matching composite substrate. If the 1.4% lattice mismatch to Fe proves to introduce excessive defects into the GaAs, Fe alloying with 12% Si would reduce the mismatch to zero(35), although alloying could have an adverse effect on grain size. Results reported for GaAs/Ge/Si solar cells suggest that mismatches of this order are not seriously detrimental to device performance, however(6).

A SrF_2 epitaxial buffer layer 0.5 μm thick is effective at blocking chemical interaction between an Fe substrate and depositing Ga and As_4 to the extent that epitaxial GaAs can be obtained. Preliminary results suggest that the insulating character of SrF_2 might be dealt with for solar cell applications by pinhole conduction to the Fe. This possibility needs to be explored more thoroughly. Alternatively, a conducting buffer layer might exist. In the search for such a material, molecularly evaporating species are preferred, since heteroepitaxial growth studies have indicated that the activation energy for the formation of mixed phases with Fe is much higher for such compounds than for dissociatively evaporating ones or for pure elements.

APPENDICES

A. Facilities Improvement

It was deemed advisable to increase the throughput and device yield of our existing thin film growth and processing facilities at the outset by adding a substrate load-lock, an *in situ* Schottky metal evaporator, and an Mo substrate holder and heater. Figure 3 is a schematic of the improved film growth facility. The "metal evaporator" station shown to the left of the analysis chamber includes an Fe source for substrate epilayers and an Au source for Schottky layers. Also, to the previously-existing complement of Knudsen cell evaporation sources in the growth chamber (Ga, As, Sn, and Si), Ge and Al sources have been added. All of the layers involved in the proposed solar cell structure, Au/GaAs/buffer layer/Fe, can now be evaporated in the same vacuum. This is important for avoiding interfacial contamination, which could interfere with substrate heteroepitaxy and also reduce Schottky device yield.

Load-lock performance is excellent: turnaround time between GaAs film growths is less than ½ hour, and theoretical electron mobility (5800 $cm^2/V's$ at 300K) has been demonstrated on GaAs films Sn- or Si-doped to the low $10^{16}/cm^3$ range, the optimum level for Schottky cells.

B. Schottky Cell Growth

For device processing, we have made metal masks with arrays of ½, 1, 2, and 4 mm holes, which can be transferred, using the load-lock, onto freshly-grown GaAs films for *in situ* evaporation of 100Å Au Schottky layers under ultra-high vacuum. Alternatively, grown films are given a controlled exposure to air and then returned to the crystal grower for Au evaporation. The latter procedure increases V_{oc} while maintaining device yield. A matching set of masks and an alignment jig has been made to apply 1 μm-thick Au contact pads to the edges of the semi-transparent Au layers; and a probe station has been set up so that diodes can be tested rapidly without requiring lead attachment. The

ELH-lamp AM1 solar simulator and the prism monochromator have been calibrated against an Eppley thermopile, the lamp for 98 mW/cm^2 and the monochromator for mW vs. photon energy from 1.0 to 3.0 eV.

Cells used in this work are 100Å Au on MBE-GaAs, with no interfacial treatment to increase V_{oc} other than just air exposure. No AR coatings are applied. This structure has been chosen for processing efficiency and reliability rather than for high power conversion efficiency, in order to facilitate performance comparison between cells grown on various substrates. Unless otherwise noted, GaAs epilayers have been grown using our standard MBE growth procedures: 1.0 μm/hr., As_4/Ga flux ratio of 2.0, 560°C substrate, and 10^{-6} Torr H_2 ambient. A ½ μm-thick n^+ layer is always grown first to insure ohmic contact.

Table II lists performance data for a cell array grown, processed, and measured as discussed above. This array was delivered to SERI on May 29, 1980. The GaAs film was exposed to air for ½ hr. before Au evaporation. Cells were measured both before and after the 160°C heating step (in air) which is required to remove the GaAs substrate from the In-wetted Mo mounting block used during MBE growth. Ideality factor, n, and forward current extrapolated to zero bias, I_o, have been calculated from the log I vs. V plots (Figure 4). Series resistance is measured at high enough forward bias to linearize the I-V curve. Shunt resistance, defined here in order to provide a comparative measure of leakage, is the slope of the I-V curve at zero bias; it has also been normalized for cell area (RA_{shunt}). All performance data in Table II are as expected for good Au/GaAs solar cells, and are very uniform from cell to cell across the surface of the 0.8 cm^2 film. Smaller cells (1 and ½ mm diameter) have also been measured on other films, and no size effect has ever been seen. It is important to note that all cells on this film are equally good, and that this has generally been true for our MBE cells; this augurs well for the scaleability of MBE to much larger cells without performance degradation. Remeasurement of two of the cells on Table II after the 160°C heating step shows increased J_o and decreased V_{oc} and FF, but such environmental instability is not of concern for these test cells.

Figure 5 shows various surface features which we have observed in MBE-GaAs and have correlated with cell performance. A typical growth surface, such as that on the cell of Table II, has an overall texture undetectably smooth by Nomarski microscopy, but is dotted with features resembling droplets and whiskers, as shown in the center of Figure 5. We have found in this work that such features have no detrimental effect on cell performance. The occasional very large growth defects which are shown to the right probably arise from pieces of contaminating matter on the substrate, and do cause cell shorting. The (211) plane, which is polar like the (111), having a Ga and an As face, is being studied in addition to the standard (100), because it is the preferential growth plane of evaporated Fe. Coarse pyramidal growth texture is observed on one face as shown to the left of Figure 5; on the other face growth is smooth, just as for (100).

Table III compares performance data for cells grown in various ways, including two grown on the coarse (indicated by ↑) and the smooth (↓) (211) faces; these faces have not been identified as to which is the Ga or As face. Both cells show mediocre diode characteristics for an unknown reason possibly related to the use of Sn doping (the Si source was not working at the time). However, the coarse-textured cell (#25) is actually better than the smooth one, suggesting that growth texture in MBE-GaAs is not important. Other data in Table III indicate the following relationships between growth parameters and cell performance:

- MBE cells have consistently higher J_{sc} than bulk GaAs cells.
- 1 μm of epitaxial GaAs (on ½ μm of n^+ epitaxy) is enough; in fact, J_{sc} is higher than for 2 μm thick cells, possibly due to a back-surface-field effect.
- Doping level in the range 2×10^{16} - $2 \times 10^{17}/cm^3$ is not critical.
- Cells made on air-exposed GaAs have less leakage (J_o and RA_{shunt}) and higher V_{oc} than those on as-grown GaAs; but the former degrade to the latter upon 160°C heating, probably due to diffusion of the oxide out of the interface.

Figure 6 shows the absolute spectral response of cell #12. Internal quantum efficiency (QE) was calculated from cell current by using published calculations of light transmission through 75Å of Au on GaAs(36).

The dotted line shows the average QE calculated as in Table II. Agreement is within 10%, and spectral response is reasonably flat. This series of experiments has established a firm base of reproducible data on MBE-GaAs Schottky cells on GaAs, against which to compare those grown on foreign substrates.

REFERENCES

1. J.C.C. Fan, C.O. Bozler, and R.L. Chapman, Appl. Phys. Lett. 32, 390 (1978).

2. Krishna P. Pande, Douglas H. Reep, Shambhu K. Shastry, Albert S. Weiner, Jose M. Borrego, and Sorab K. Ghandhi, IEEE Trans. on Electron Devices, ED-27, 635 (1980).

3. W.D. Johnston, Jr., H.J. Leamy, B.A. Parkinson, A. Heller, and B. Miller, J. Electrochem. Soc. 127, 90 (1980).

4. K. Pande, D. Reep, A. Srivastava, S. Tiwari, J.M. Borrego, and S.K. Ghandhi, J. Electrochem. Soc. 126, 300 (1976).

5. Shirley S. Chu, Ting L. Chu, and Yao T. Lee, IEEE Trans. on Electron Devices, Ed-27, 640 (1980).

6. B.Y. Tsaur, M.W. Geis, John C.C. Fan, and R.P. Gale, Appl. Phys. Lett. 38, 779 (1981).

7. B.A. Movchan and A.V. Demchishin, Fiz. Metall. Metalloved., 28, 653 (1969).

8. A.R. Calawa, Appl. Phys. Lett. 33, 1020 (1978).

9. John C.C. Fan, A.R. Calawa, Ralph L. Chapman, and George W. Turner, Appl. Phys. Lett. 35, 804 (1979).

10. D.L. Miller and J.S. Harris, Jr., Appl. Phys. Lett. 37, 1104 (1980).

11. C.Y. Chang, Y.K. Fang, and S.M. Sze, Solid State Electronics 14, 541 (1971).

12. M. Illegems, J. Appl. Phys. 48, 1278 (1977).

13. Toshihisa Suzuki, Makoto Konagai, and Kiyoshi Takahashi, Thin Solid Films, 60, 85 (1979).

14. A.Y. Cho, J. Appl. Phys. 46, 1733 (1975).

15. Donald L. Smith, unpublished work.

16. Hideki Hasegawa, Kiyoaki Kojima, and Takamasa Sakai, Japan, J. Appl. Phys. 16, 1251 (1977).

17. D.L. Partin, A.G. Milnes, and L.F. Vassamillet, J. Electronic Materials 7, 279 (1978).

18. T.C. Reiley and W.D. Nix, Metallug. Trans. 7A, 1695 (1976).

19. William F. Weston, Thomas C. Baker, Carl J. Smith, Abraham L. Chavez, Virgil K. Grotzky, and James F. Capes, J. Vac. Sci. Technol. 15, 54 (1978).

20. W. Hume-Rothery and G.V. Raynor, The Structure of Metals and Alloys, p. 267 (Inst. of Metals, London, 1962).

21. Analysis carried out by Paul S. Prevey of Metcut Research Associates, Cincinnati, Ohio (1977), now of Lambda Research, Inc., Cincinnati, Ohio.

22. K. Kennedy, Trans. of the Internat. Vacuum Metallurgy Conf. (American Vacuum Society, N.Y., 1968), p. 195.

23. D.L. Smith and V.Y. Pickhardt, J. Appl. Phys., 46, 2366 (1975).

24. J.R. Waldrop and R.W. Grant, Appl. Phys, Lett. 34, 630 (1979).

25. G.A. Prinz and J.J. Krebs, Appl. Phys. Lett. 39, 397 (1981).

26. C. Russo and R. Kaplow, Surf. Sci. 69, 453 (1977).

27. L.L. Chang, A. Segmuller, and L. Esaki, Appl. Phys. Lett. 28, 39 (1976).

28. P.M. Petroff, A.C. Gossard, A. Savage, and W. Wiegmann, J. Cryst. Growth 46, 172 (1979).

29. A.C. Gossard in Thin Film: Preparation and Properties, K.N. Tu and R. Rosenberg, eds (Academic Press, to be published).

30. Chin-An Chang, Armin Segmuller, L.L. Chang, and L. Esaki, Appl. Phys. Lett. 38, 912 (1981).

31. R.S. Bauer and J.C. McMenamin, J. Vac. Sci. Technol., 15, 1444 (1978).

32. J.C. Phillips, J. Vac, Sci. Technol. 19, 545 (1981).

33. R.F.C. Farrow, P.W. Sullivan, G.M. Williams, G.R. Jones, and D.C. Cameron, J. Vac. Sci. Technol., 19, 415 (1981).

34. Max Hansen, Constitution of Binary Alloys (McGraw-Hill, N.Y., 1958).

35. Richard M. Bozorth, Ferromagnetism, p. 74 (Van Nostrand, Princeton, N.J., 1951).

36. R.J. Stirn, and Y.M. Yeh, Conf. Rec. IEEE Photo. Spec. Conf., 10th, Palo Alto, p. 15 (1973).

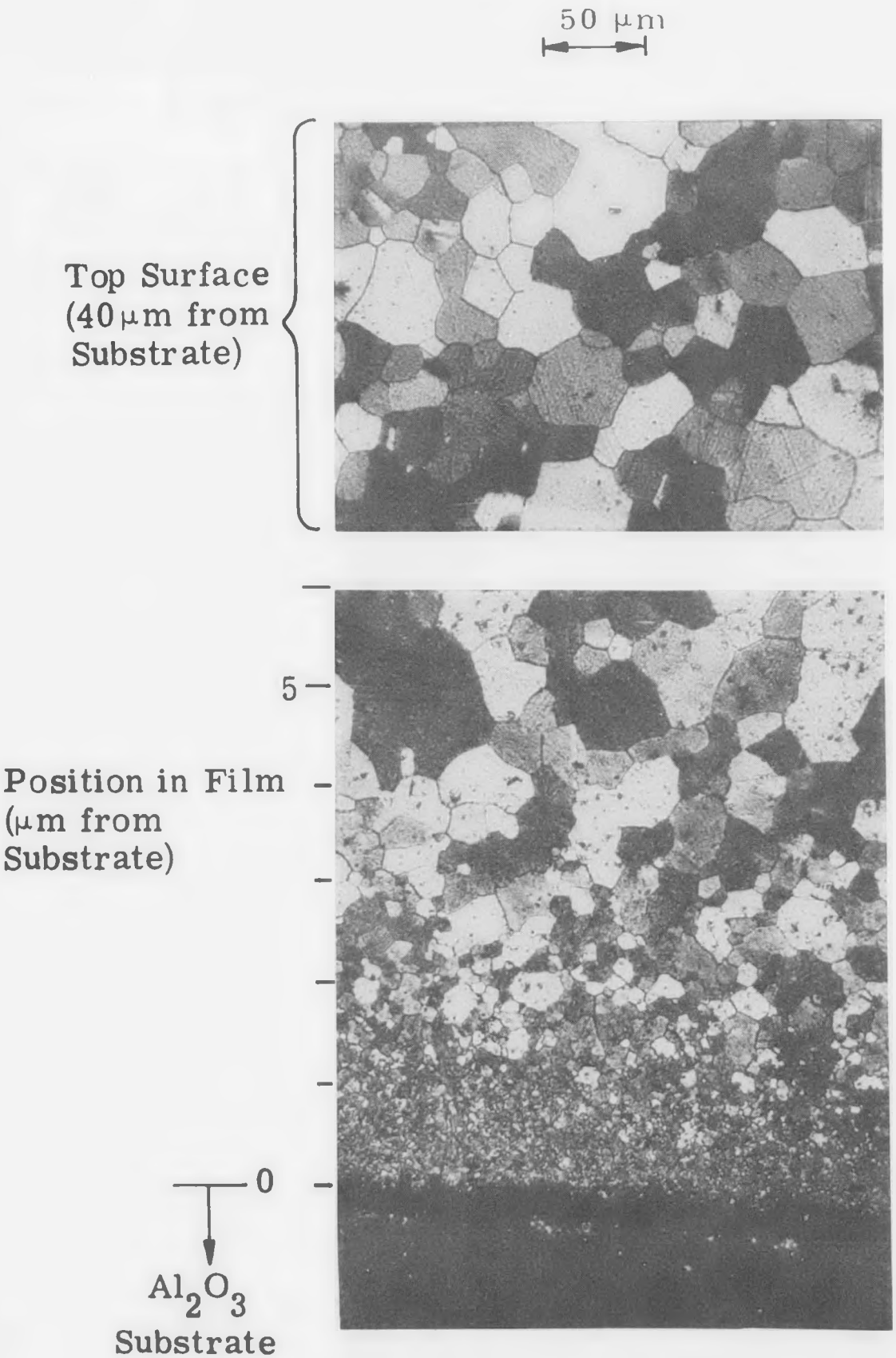

FIGURE 1. Angle-lapped cross-section of Fe film on alumina.

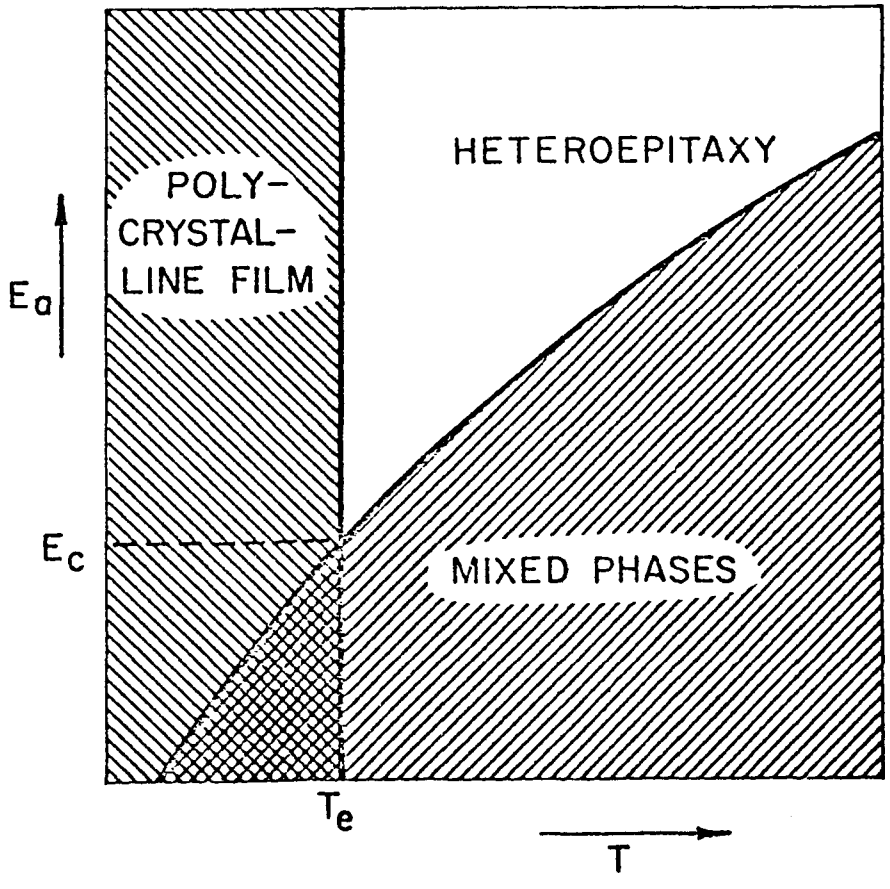

Figure 2. Generalized heterepitaxial growth behvaior.

E_a = activation energy for formation of mixed phases at growth interface; T = growth temperature

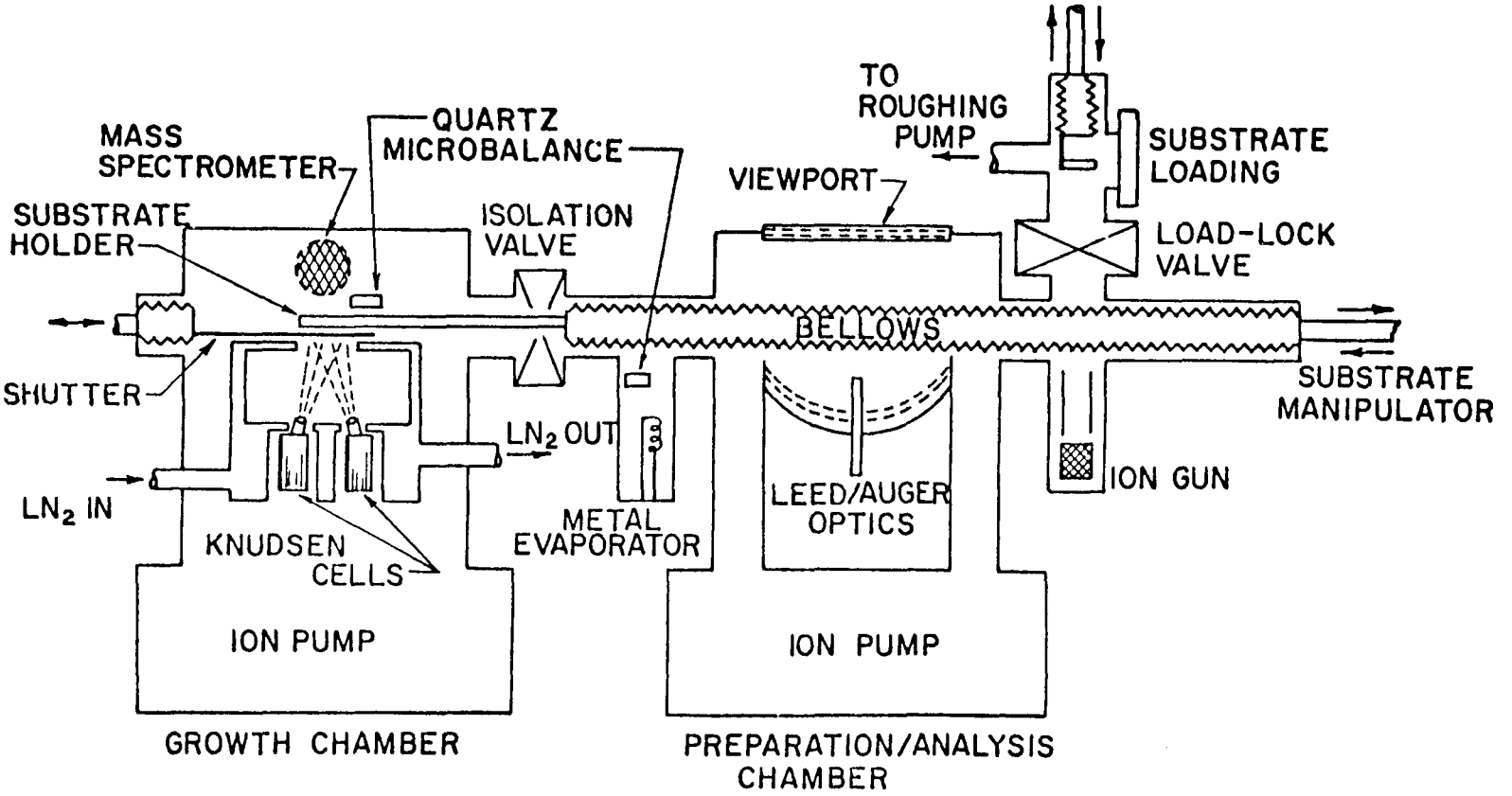

FIGURE 3. OVERALL SCHEMATIC OF MBE SYSTEM

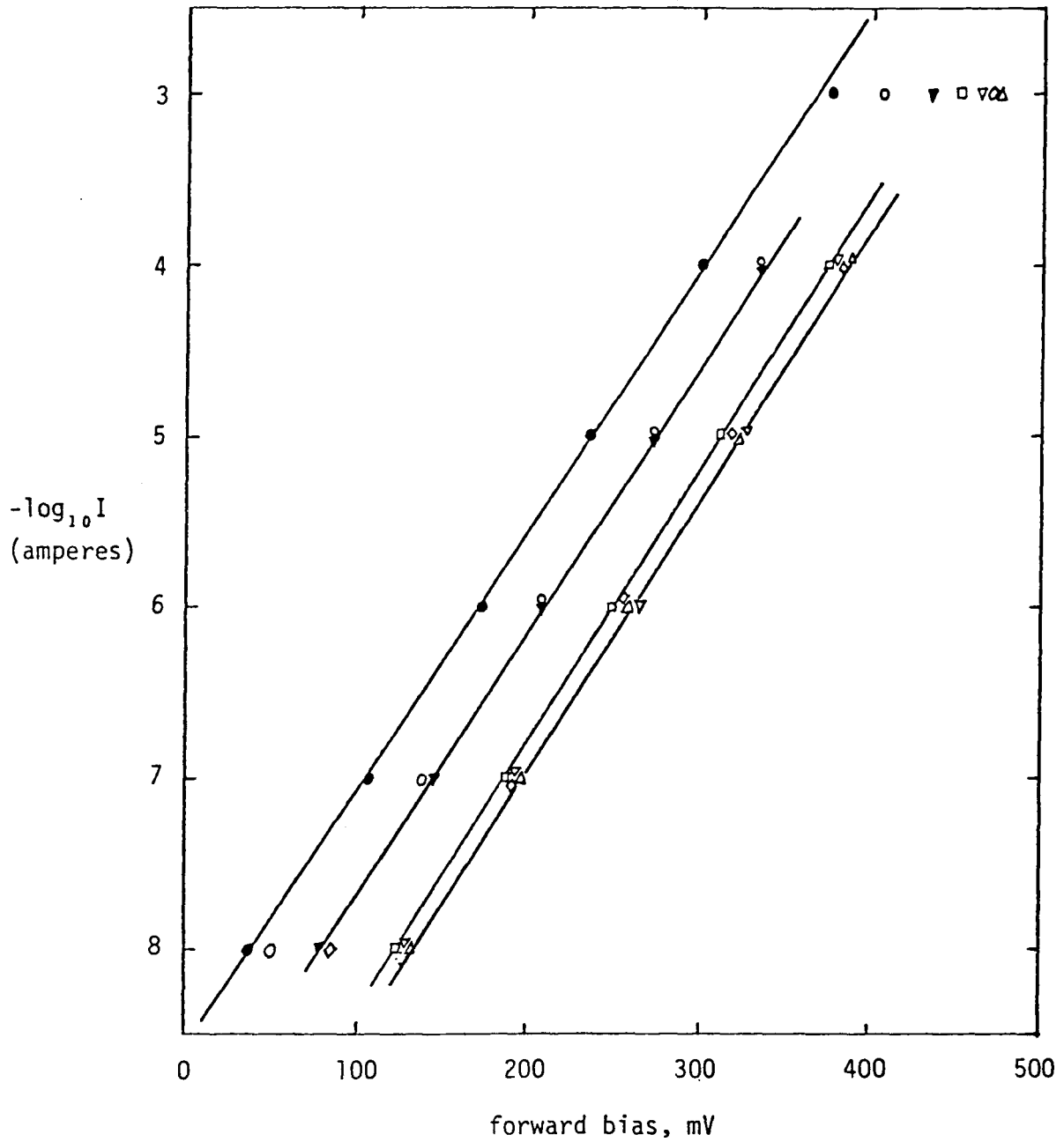

Figure 4. Forward characteristics of cells on Film #27. 100Å Au.
open symbols - before 160°C heating, solid symbols - after; diode numbers (refer to data table): (o)=4,(▽)=2a,(◇)=2b,(△)=2c,(□)=2d.

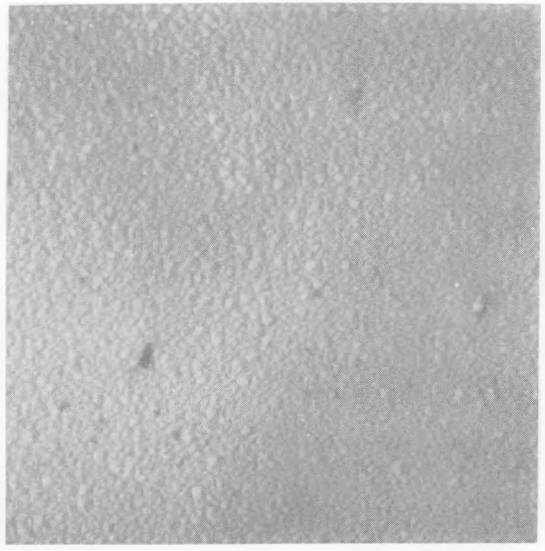

(2II) GROWTH PLANE,
"WRONG" POLARITY

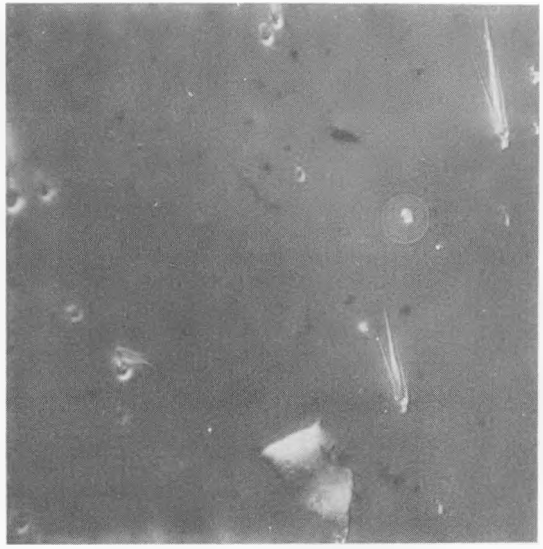

TYPICAL GROWTH SURFACE
YIELDING EXCELLENT
SCHOTTKY CELLS

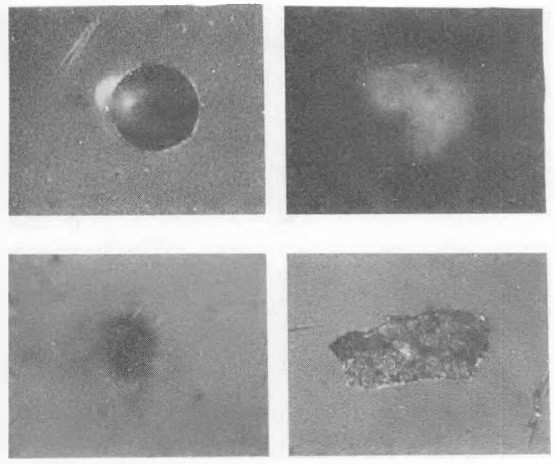

VARIOUS GROWTH DEFECTS
CAUSING SCHOTTKY CELL
DEGRADATION

FIGURE 5 NOMARSKI MICROGRAPHS OF VARIOUS MBE -GaAs GROWTH SURFACES

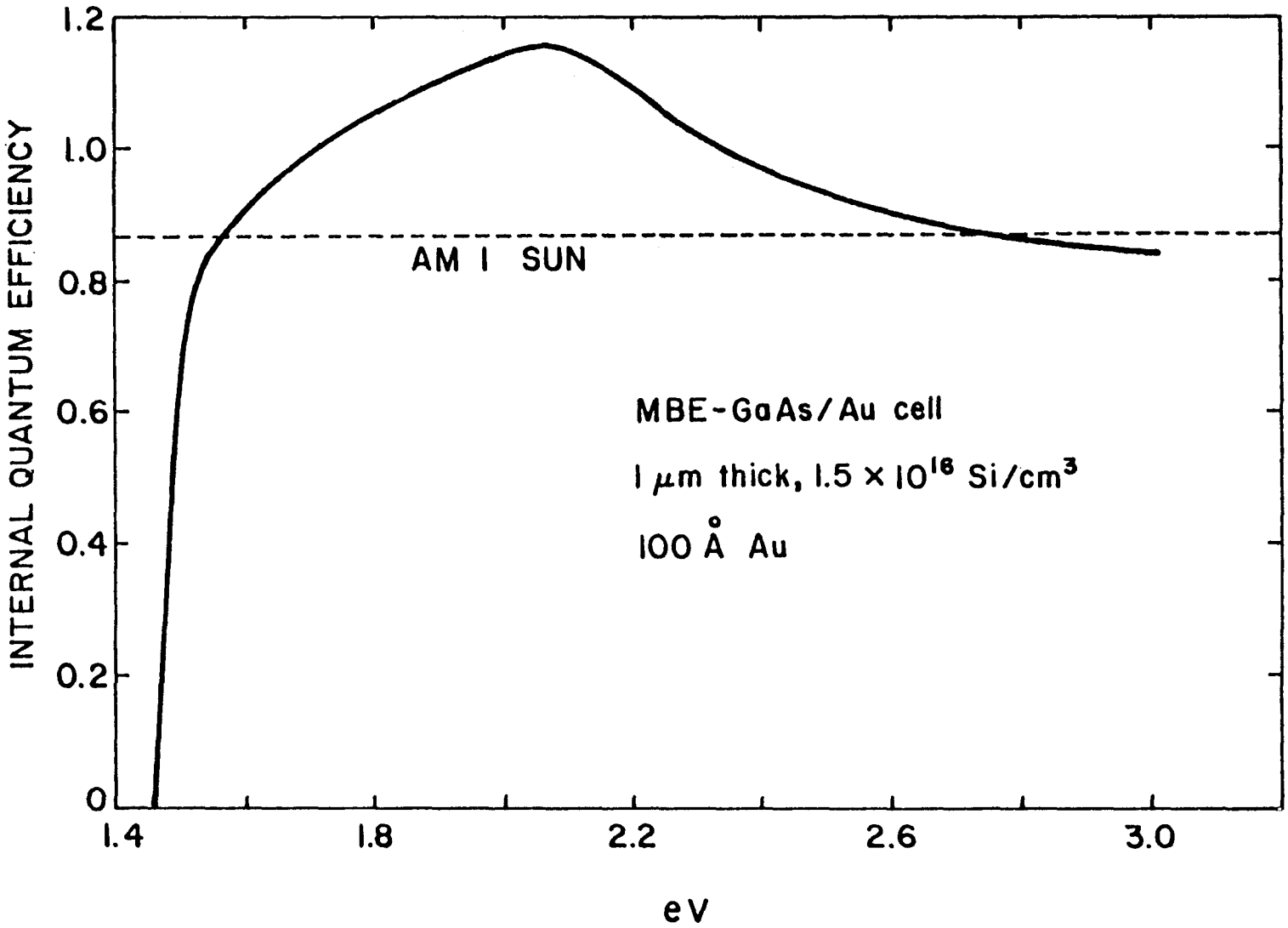

FIGURE 6 ABSOLUTE SPECTRAL RESPONSE OF CELL #12

TABLE I.

Buffer Layer Growth Summary

buffer material	Δa vs. GaAs, % at 25°C	cubic structure type	epitaxy on Fe (by LEED) result	growth T,°C.	film thickness, μm	Fe in Auger, μV(a)	GaAs epitaxy on buffer result	growth T,°C	GaAs thickness, μm	buffer in Auger, μV (a)
(Fe)	+1.4	body-centered					no	(see GaAs on Fe)		
(GaAs)	-	zinc-blende	no	400 460 560 600	0.1 0.1 0.1 0.6 0.06	0 0 0.6 0 1.2				
AlAs	-0.2	zinc-blende	no	400 600	0.05 0.3 0.1	1.5 0	yes	see ref. (27)		
Ge(b)	+0.1	diamond	no	300 400 430 500 600	0.1 0.1 0.1 0.1 0.1-0.9	0 0 2.6	yes	see ref. (28)		
Cr	+2.0	body-centered	yes	400 600	0.027 0.06	0 0.7	no	400 450 500 560	0.25 0.1 0.1 0.1	0 0-0.3 0.5 0.15 (c)
SrF_2	+2.3	fluorite	yes	400 400 600 600	0.1 0.5 0.1 0.5	0.4 0 1.0 0	yes	540 600	1.0-2.5	0

a) Auger peak heights for the pure materials were 3.7 μV for Fe(651 eV) and 7.5 μV for Cr(529 eV).
b) Also on Cr/Fe; see text.
c) +.0.2 μV Fe; Cr only 0.027 μm thick.

TABLE II. Schottky Cell Performance Data

film # * 27		before 160° heating						after	
description		1.0 μm GaAs, 7×10^{16} Si/cm^3, on GaAs(100): 100Å Au							
diode dia.(mm), pos.*		4	2a	2b	2c	2d		4	2a
net A, cm^2 (contact less)		0.125	.031	.030	.031	.031		0.125	.031
dark	n	1.11	1.07	1.09	1.09	1.07		1.11	1.11
dark	I_o(A)	8×10^{-10}	1.2×10^{-10}	1.0×10^{-10}	1.0×10^{-10}	1.2×10^{-10}		2.5×10^{-9}	8×10^{-10}
dark	J_o(A/cm^2)	6×10^{-9}	4×10^{-9}	3×10^{-9}	3×10^{-9}	4×10^{-9}		2.0×10^{-8}	2.6×10^{-8}
$R_{ser.}(\Omega)$= $\Delta V/\Delta I$ fwd.	dark								
$R_{ser.}(\Omega)$= $\Delta V/\Delta I$ fwd.	AM1	4	11	7	9	8		7	12
$R_{shunt}(\Omega)$= $\Delta V/\Delta I\|_{V=0}$	dark								
$R_{shunt}(\Omega)$= $\Delta V/\Delta I\|_{V=0}$	AM1	20K	67K	67K	67K	50K		10K	40K
$RA_{shunt.}$ AM1 (Ω-cm^2)		2500	2100	2000	2100	1600		1300	1200
AM1 (ELH lamp)	V_{oc} (V)	0.41	0.40	0.40	0.39	0.40		0.36	0.35
AM1 (ELH lamp)	I_{sc} (μA)	1400	350	350	345	340		1300	310
AM1 (ELH lamp)	V_p (V)	0.33	0.32	0.32	0.32	0.32		0.30	0.27
AM1 (ELH lamp)	I_p (μA)	1300	320	320	320	310		1100	270
AM1 (ELH lamp)	J_{sc}(mA/cm^2)	11.2	11.3	11.3	11.1	11.0		10.0	10.0
AM1 (ELH lamp)	$QE_{int.}$(%) **	86	87	87	85	85		77	77
AM1 (ELH lamp)	FF	.75	.73	.73	.76	.73		.70	.67

* film # and diode position indexing as shown ——→

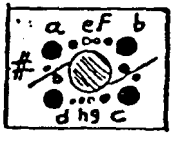

** assumes 13mA/cm^2 (29mA/cm^2 x 0.45 average transmission through Au) for QE=100%, from data in H.J. Hovel, "Solar Cells", p. 119 (Academic, 1975)

TABLE III. COMPARISON OF MBE - GaAs/100Å Au SCHOTTKY CELLS GROWN ON n+ - GaAs

CELL NO.	GROWTH PLANE	THICKNESS, MICRONS	DOPANT, N/CM³	Au INTERFACE TREATMENT	160°C HEAT BEFORE MEASURING?	n	Jo, A/CM²	SHUNT RA, OHM-CM²	V_{OC}	Jsc, MA/CM²	FF
9	(100)	(BULK)	Si 1×10^{17}	ACID-CLEAN	NO	1.06	7×10^{-10}	2000	.42	7.3	.68
10	↓	2	2×10^{16}	VACUUM	NO	1.12	1×10^{-8}	380	.37	10.4	.67
11	↓	↓	↓	1 DAY AIR	NO	1.08	2×10^{-9}	1200	.42	10.8	.74
11	↓	↓	↓	" "	YES	1.05	2×10^{-8}	1200	.36	9.5	.68
12	↓	1	↓	10 MIN. AIR	NO	1.1	4×10^{-9}	1000	.41	11.3	.74
13	↓	↓	2×10^{17}	↓	NO	1.1	5×10^{-8}	2500	.35	10.5	.73
25	(211)↑	1½	Sn 5×10^{16}		YES	1.9	3×10^{-6}	380	.35	9.2	.62
26	(211)↓	↓	↓		YES	2.2	3×10^{-5}	190	.32	9.1	.51

TABLE IV. SURFACE PASSIVATION OF Fe

GAS	Fe TREATMENT °C	Fe TREATMENT Torr	sec.	GaAs GROWTH °C	GaAs GROWTH μm	LEED*	Fe, 651eV	AUGER, μV N,S	AUGER, μV Ga	AUGER, μV As
						E	3.7			
NH_3	350	760	10			N	2.1	3.9		
	450		300			W	2.4	1.6		
			10			E→W	2.8	1.3→2.1		
				450	$3E16As_4/cm^2$	N	1.6	0.3		0.4
				450	0.1	N	0.4	1.6	0.4	0.4
H_2S	450	1	10			N	0.9	48		
		0.1				E	2.5	38		
				450	$3E16As_4/cm^2$	E-W				
					0.16	N	0	13	0.4	0.2
	600	10				N	0.4	60		
		1				E-W				
				550	0.1	N	0.5	6.0	0.2	0.3

* E = epitaxial, W = weak, N = none